Shock Waves (1999) 9: 73–79

Shock Waves

Numerical simulations of nozzle starting process

T. Saito[1], K. Takayama[2]

[1] Nihon Silicon Graphics·Cray K.K., Institute of Fluid Science, Supercomputer Center, Tohoku University, 2-1-1 Katahira, Sendai, 980-8577 Japan
[2] Shock Wave Research Center, Institute of Fluid Science, Tohoku University, 2-1-1 Katahira, Sendai, 980-8577 Japan

Received 16 June 1998 / Accepted 17 August 1998

Abstract. The starting process of two-dimensional nozzle flow is investigated both experimentally and numerically. Discussions are made on the comparison between experimental and numerical results. Performances of two numerical methods which are used in the present study of unsteady flow problem are also discussed and indications for future development of numerical tools to study nozzle problems are obtained.

Key words: Shock wave, Boundary layer, Nozzle flow, Numerical simulation

1 Introduction

The progress in the computational fluid dynamics (CFD) due to implementations of TVD stability conditions made in early 1980's contributed much to the study of shock wave phenomena as well as many other area of fluid dynamics (Harten 1983). The TVD schemes provide higher resolutions of discontinuities such as shock waves and contact surfaces without unphysical oscillations compared with traditional numerical schemes. As a result, together with the development of high performance computers, detailed investigations of unsteady fluid flow are now possible.

The theoretical developments, however, on the properties of numerical schemes such as accuracy and stability are established, in most cases, for linear scaler problems. Therefore it is still important to verify limitations and applicabilities of numerical schemes for each specific case by comparing them with reliable experimental data.

The gas behind the reflected shock wave at the shock-tube end wall is expanded to high flow Mach numbers in nozzles. The process starting with the incident shock wave entering the nozzle until a quasi-steady flow is achieved is called the starting process of the nozzle. The starting process has been investigated by many researchers (Smith 1966, Amann 1969). The starting process was also investigated numerically by Prodromou and Hillier (1991). Although they made some part of the starting process, especially the very beginning of it, clear by comparing the numerical results with experimental data, one of the conclusions is that it is necessary to include viscous effect in the numerical analysis in order to simulate details of the process such as the interactions of the shock waves and boundary layers. In the current study, the starting process of a two-dimensional nozzle is calculated by solving the full Navier-Stokes equations and the results are compared with experimental data obtained by the method of double exposure laser holographic interferometry.

Detailed investigations of the starting process of nozzle flow is necessary for developing high performance equipments generating hypersonic flows. This study started in conjunction to the project of developing a high performance shock-tunnel at the Shock Wave Research Center (SWRC), Tohoku University.

Correspondence to: T. Saito

2 Numerical simulation

In this study, the full Navier-Stokes equations are solved by using two different numerical schemes. One of them is the explicit upwind TVD scheme of Harten and Yee and the other is an implicit scheme, LUSGS (Lower Upper Symmetric Gauss Siedel scheme). Both schemes are coded for structured meshes in general curvilinear coordinates.

2.1 Governing equations

The two dimensional time dependent equations for viscous, heat-conducting flow in Cartesian coordinates are given in a conservative vector form by:

$$U_t + F_x + G_y = F_{v_x} + G_{v_y}. \tag{1}$$

where t, x and y are the time and space coordinates (Anderson 1984). The vector of conserved quantities, U, is of the following form:

$$U = \begin{pmatrix} \rho \\ \rho u \\ \rho v \\ E \end{pmatrix}, \tag{2}$$

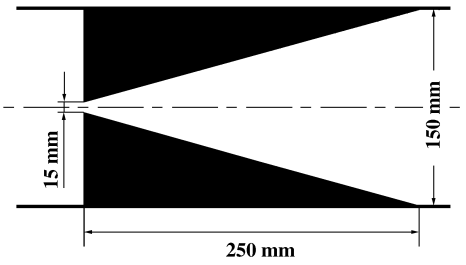

Fig. 1. Dimensions of 2-D nozzle

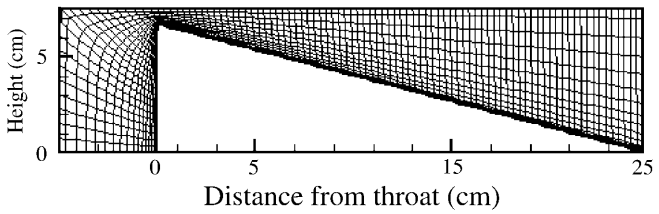

Fig. 2. Numerical grid of the nozzle (schematic)

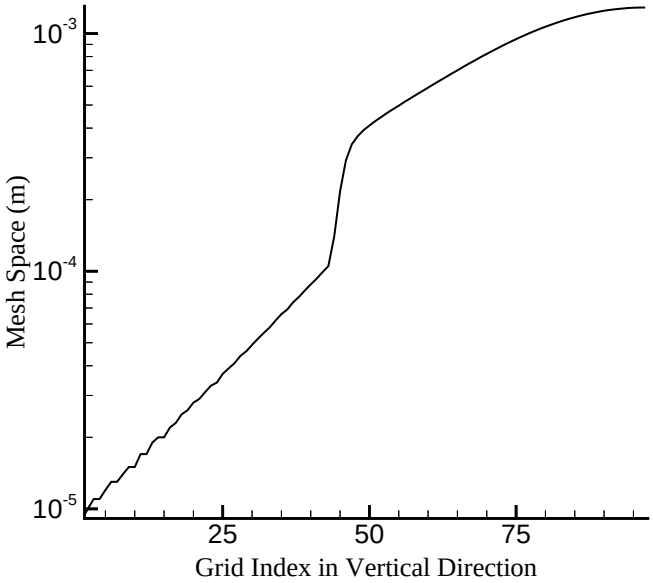

Fig. 3. Space between grid points

and the convection terms, F and G, are expressed as:

$$F = \begin{pmatrix} \rho u \\ \rho u^2 + p \\ \rho uv \\ (E+p)u \end{pmatrix}, \quad G = \begin{pmatrix} \rho v \\ \rho uv \\ \rho v^2 + p \\ (E+p)v \end{pmatrix}, \qquad (3)$$

where ρ, p, u, v are the density, pressure, flow velocity elements in x and y directions, respectively. The total energy per unit volume, E, is expressed as $E = \rho\epsilon + \rho(u^2+v^2)/2$ and an ideal-gas equation of state, $\epsilon = p/(\gamma+1)\rho$, is used to close the whole system of equations. Here γ is the ratio of specific heats of the gas.

The viscous terms, F_v and G_v are given by:

$$F_v = \begin{pmatrix} 0 \\ \tau_{xx} \\ \tau_{xy} \\ u\tau_{xx} + v\tau_{xy} - q_x \end{pmatrix}, G_v = \begin{pmatrix} 0 \\ \tau_{xy} \\ \tau_{yy} \\ u\tau_{xy} + v\tau_{yy} - q_y \end{pmatrix}, \qquad (4)$$

where the viscous stress tensors are expressed as:

$$\tau_{xx} = \frac{2}{3}\mu\left(2\frac{\partial u}{\partial x} - \frac{\partial v}{\partial y}\right), \quad \tau_{yy} = \frac{2}{3}\mu\left(2\frac{\partial v}{\partial y} - \frac{\partial u}{\partial x}\right),$$

$$\tau_{xy} = \tau_{yx} = \mu\left(\frac{\partial u}{\partial y} + \frac{\partial v}{\partial x}\right),$$

where μ is the coefficient of viscosity and q is the heat transfer per unit volume per unit time. In actual computations, the equations in general curvilinear coordinates are used. The equations are further transformed into computational index space and nondimensionalized following the standard process.

2.2 Numerical schemes

Implicit schemes are usually used for solving basic flow equations for steady problems since they have high stabilities for large time steps. For transient flow problems, however, consecutive flow fields with relatively small time intervals are sought. Especially in cases which deal with complex wave interactions such as present study, time steps can not be too large even if the scheme itself is stable. Implicit schemes usually takes much more CPU time to calculate each time step compared with typical explicit schemes. Therefore implicit schemes are not so efficient for unsteady problems. In the current study, an implicit scheme of LUSGS and an explicit TVD scheme of Harten-Yee are used to investigate the benefits of each scheme when applied to time-dependent shock interaction problems.

Details of LUSGS scheme which is used in this paper are not described here. The method follows standard processes and the details are found elsewhere (Yoon and Jameson 1988; Kano et al. 1995). The only thing which is specific to this problem is that the viscous terms are included in the explicit terms only. The terms related to the flux Jacobians which appear in rigorous formulations are left out. The omission of these viscous Jacobian terms make the matrix inversion unnecessary. Accordingly, the scheme becomes much simple and fast to run. The Crank-Nicholson scheme is used to obtain second-order time-accuracy and solutions are obtained by Newton-iteration at each time step. Therefore the spatial-accuracy of the solution is determined by the explicit terms which are based on second-order Harten-Yee TVD schemes. When the solution is converged, the effect of viscosity is properly included despite the fact that the viscous Jacobian terms are neglected.

The explicit code is based on the upwind TVD scheme of Harten (1983) and Yee (1987). Strang type operator splitting (Strang 1968) is employed to handle multi-dimensional calculations and the viscous terms are included in each split directions. The alternative, perhaps, is to include the viscous terms only once at each time step. However, although detailed investigations are not carried out, the differences both in the solutions and in CPU time due

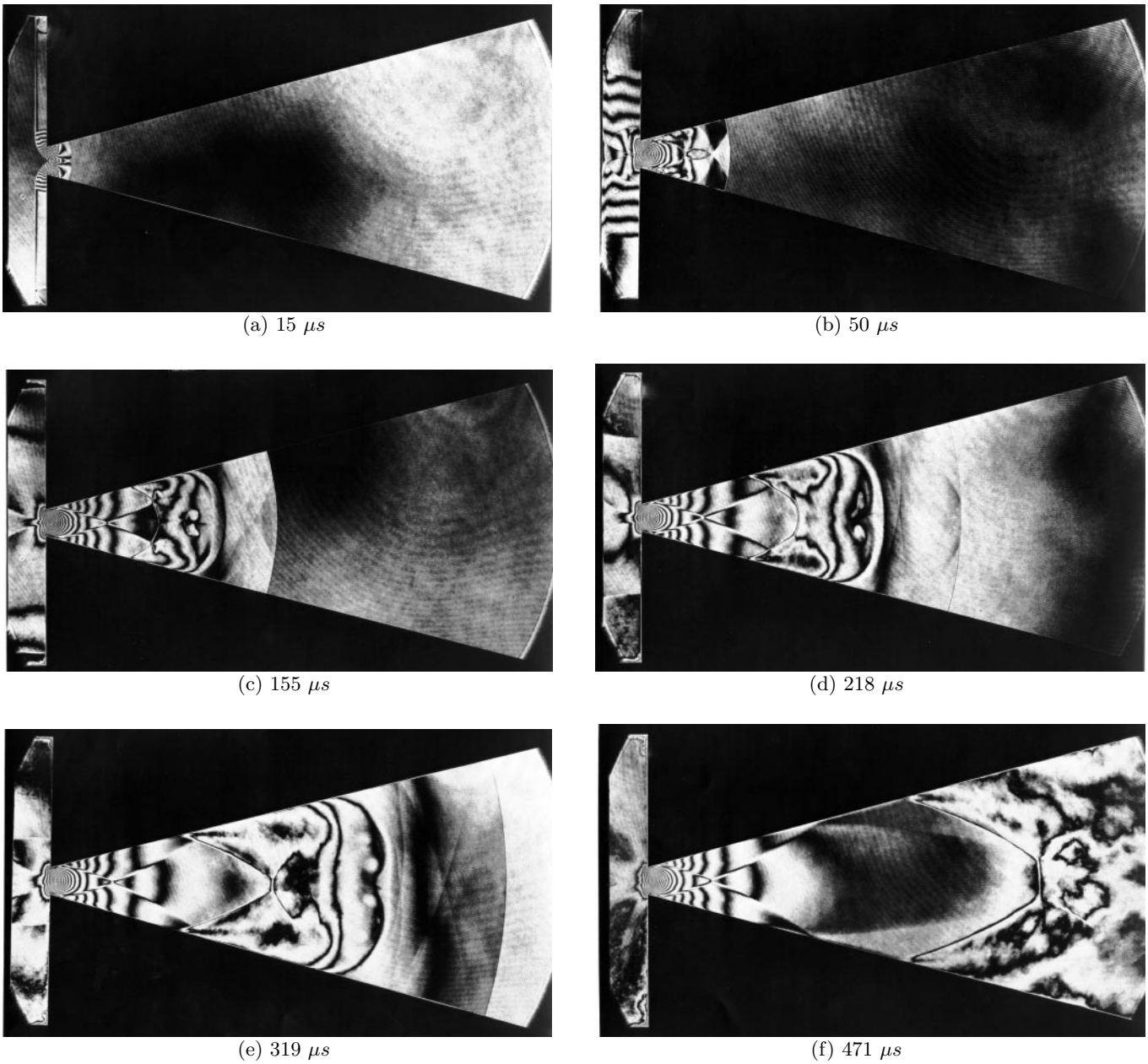

(a) 15 μs (b) 50 μs

(c) 155 μs (d) 218 μs

(e) 319 μs (f) 471 μs

Fig. 4a–f. Experimental results

to different ways of including viscous terms are expected to be negligibly small. As is usually done, Roe's approximate Riemann solvers are used and the minmod TVD limiter with artificial compression is used in the current study in order to avoid numerical oscillations while minimizing the diffusion of each wave front. The scheme has second-order accuracy both in space away from solution's singularities and in time.

2.3 Grid generation

A reflection nozzle was placed at the end of the rectangular-cross-section (60mm $\times$ 150mm) shock tube as schematically shown in Fig. 1.

A numerical grid of the nozzle is generated for the numerical simulations and is shown in Fig. 2 with reduced numbers of grid lines for clarity. The number of nodes is 600 x 100. The numerical grids are contracted toward the solid wall by using the following formula proposed by Roberts (1971),

$$y = \frac{h(\beta+1) - (\beta-1)\{[(\beta+1)/(\beta-1)]^{1-\bar{y}}\}}{[(\beta+1)/(\beta-1)]^{1-\bar{y}} + 1} \ ,$$

where $\bar{y}$ is the value obtained by dividing the node number counted from the wall by the total number of grid points in the y direction. The parameter β is the stretching parameter which takes values greater than unity. The grid points are clustered more for smaller values of β.

Table 1. Initial and boundary conditions

		Shock tube	Nozzle
Pressure	(Pa)	1.05×10^5	1.47×10^4
Density	(Kg/m^3)	5.93×10^{-1}	1.78×10^{-1}
Flow velocity	(m/s)	5.96×10^2	0
Sound speed	(m/s)	4.98×10^2	3.40×10^2
Temperature	(K)	6.16×10^2	2.88×10^2

The grid spacings measured at the middle of the nozzle are plotted in Fig. 3. The space between the wall and the adjacent grid point is about 10 μm and is small enough to resolve details of the boundary layer for the current study. The same numerical grid is used for the two numerical schemes.

2.4 Initial and boundary conditions

Calculations are carried out only for the lower half of the nozzle due to symmetry of the flow. The initial conditions correspond to the moment when a plane incident shock wave with Mach number of 2.5 reaches to the shock-tube end wall where the nozzle entrance is located. The test gas is air with $\gamma = 1.4$, and the initial flow conditions are listed in Table 1.

In the present calculations, it is assumed that the coefficient of viscosity is dependent only on the temperature and follows Sutherland viscosity law:

$$\frac{\mu}{\mu_0} = \left(\frac{T}{T_0}\right)^{\frac{3}{2}} \frac{T_0 + S_1}{T + S_1},$$

where S_1 is a constant value of 110 K and μ_0 is the coefficient of viscosity at a reference state. The value of 1.79×10^{-5} $Pa \cdot s$ is used for μ_0. The constant value of 0.72 for the Plandtl number is also assumed. The non-slip boundary condition is used on solid walls and the wall temperature is kept at the room temperature of 288 K.

3 Experimental results

A series of experiments with the conditions listed in Table 1 was carried out in order to investigate the initial transient flow in the nozzle. The flow is visualized by using the double exposure laser holographic interferometry. The results are shown in Figs. 4(a) to (f) corresponding to different times from the moment of arrival of the incident shock wave at the nozzle throat.

On the arrival of incident shock wave, upper and lower parts of the incident shock wave are reflected at the shock-tube end wall and propagates back away from the wall leaving behind a stationary high pressure region. The incident shock wave at the nozzle throat, on the other hand, is transmitted unchanged. As a result, shock waves, transverse to the main flow, are created at the upper and lower edges of the nozzle throat and propagate towards the plane of symmetry. The two shock waves soon collide at the plane of symmetry and transmitted with each other, Fig. 4(a). This can also be considered as reflections of the shock waves at an imaginary solid plane replacing the plane of symmetry. The symmetric nature of the flow is kept quite well as seen in the series of pictures in Fig. 4 which justifies the assumed symmetry of the flow in the numerical calculations.

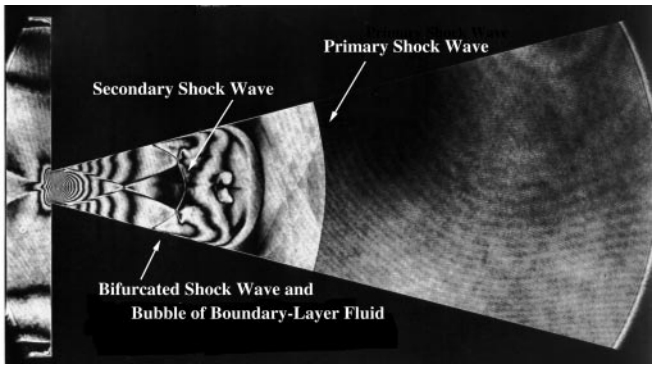

Fig. 5. Experimental result at 155μs

The transverse shock waves repeat reflections between the nozzle walls behind the primary transmitting shock wave. Soon a secondary shock wave is generated and the flow field increases its complexity. Due to interactions with the boundary layers, the secondary shock wave is bifurcated at the wall creating bubbles of boundary layer fluid as seen in Fig. 4. and Fig. 5 which is an enlarged image of Fig. 4(c).

4 Numerical results and discussions

Figure 6 shows the holographic images of the density field corresponding to times of experimental results obtained by the explicit scheme of Harten and Yee.

Figure 7 is the density contour lines in the x-t plane recorded at the plane of symmetry. It is noted that, at about 2 cm from the nozzle throat, a left-running secondary shock wave is clearly formed and is carried to the right because of the supersonic counter flow.

Bifurcations of the secondary shock wave at the nozzle walls are clearly seen together with the formation of bubbles at the foot of bifurcated portions of the shock wave. The mechanism of the bifurcation was investigated by Mark (1958) using a shock tube as a study of interaction of the boundary layer induced behind the incident shock wave and the shock wave reflected at the end wall. In the current nozzle flow problem, in addition to the simple shock tube case, interactions of transverse waves and diverging geometry make the flow field more complex. Although the detailed shapes and positions do not match exactly, the creation of vortices behind the interface which separates gases originally came from the upstream and the downstream of the nozzle throat is seen. The mechanism of vortex creation and complex wave interactions in the region between the primary and the secondary shock waves are analyzed by Amann (1968; 1971) and the source of the vortices is found to be the large differences in the

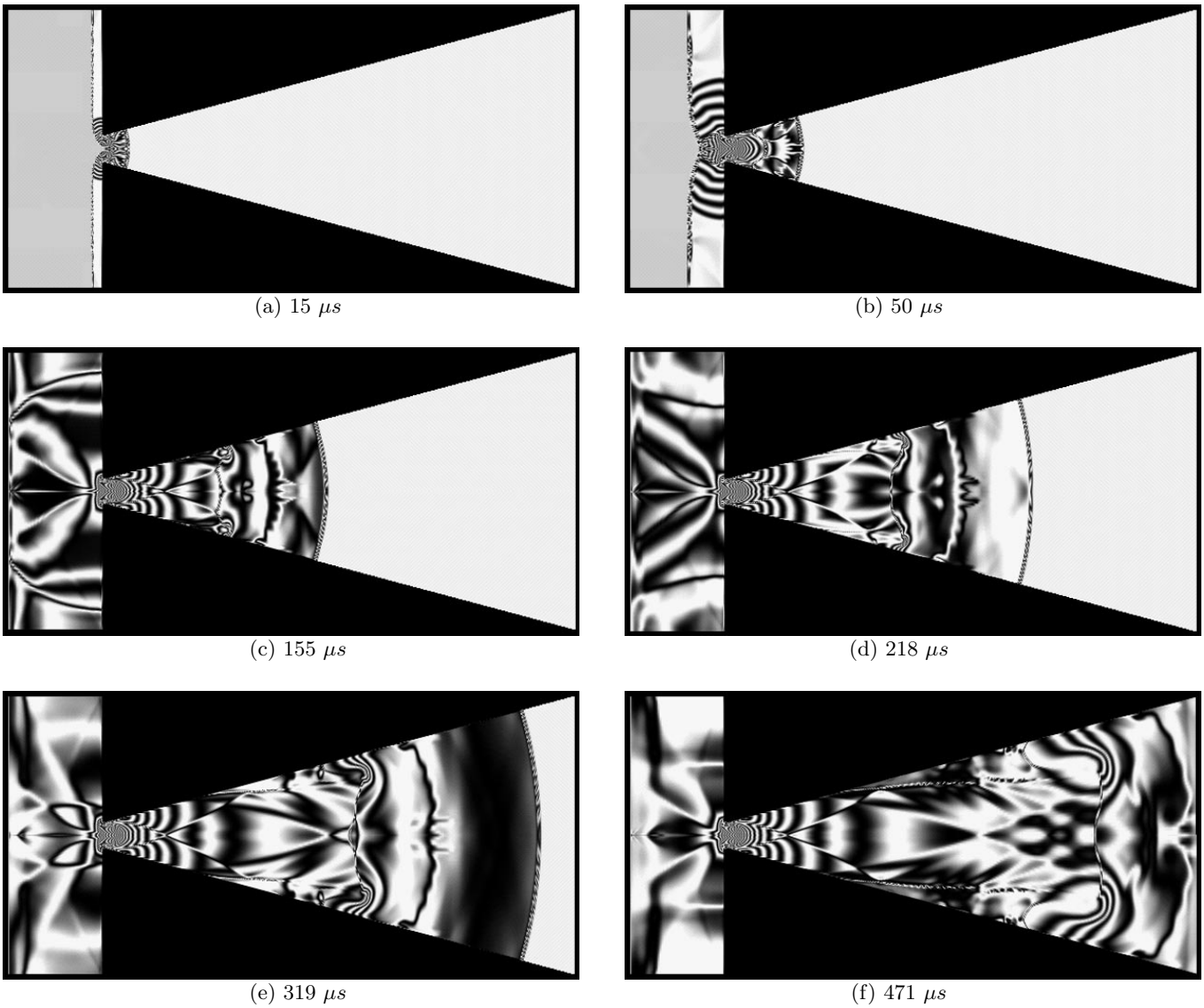

(a) 15 μs (b) 50 μs

(c) 155 μs (d) 218 μs

(e) 319 μs (f) 471 μs

Fig. 6a–f. Numerical results (explicit calculations)

tangential velocity at the interface. A series of animation was made using 400 numerically obtained interference images. The creation and the time evolution of vortices are observed more clearly in the animation.

The agreement between the experimental and the numerical results is quite good from the beginning to about 218 μs, (a) to (d) of Figs. 4 and 6. Then the numerically obtained flow field starts to deviate from that of experiment. Most noticeable difference is the grow rate of the bubble of the boundary-layer fluid. It becomes larger in the numerical results compared with those of the experiment. This is most likely the result of the current laminar calculations. It is pointed out by Mark that the shock bifurcation is suppressed once the boundary layer becomes turbulent. Accordingly, the growth of the bubble is also suppressed. Another evidence that the boundary layer being turbulent in the experiment is that the flow separation is clearly seen in the numerical results, Figs. 6(e) and (f), while in the experiment, the flow is still attached to the nozzle walls without clear signs of boundary layer separations. Although it is difficult to clearly define the Reynolds

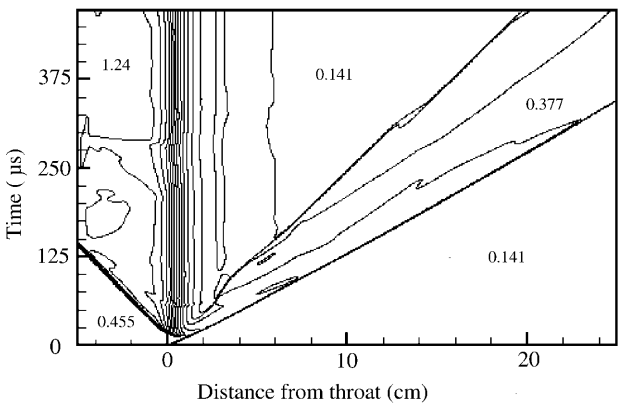

Fig. 7. Isophcnics in x-t plane

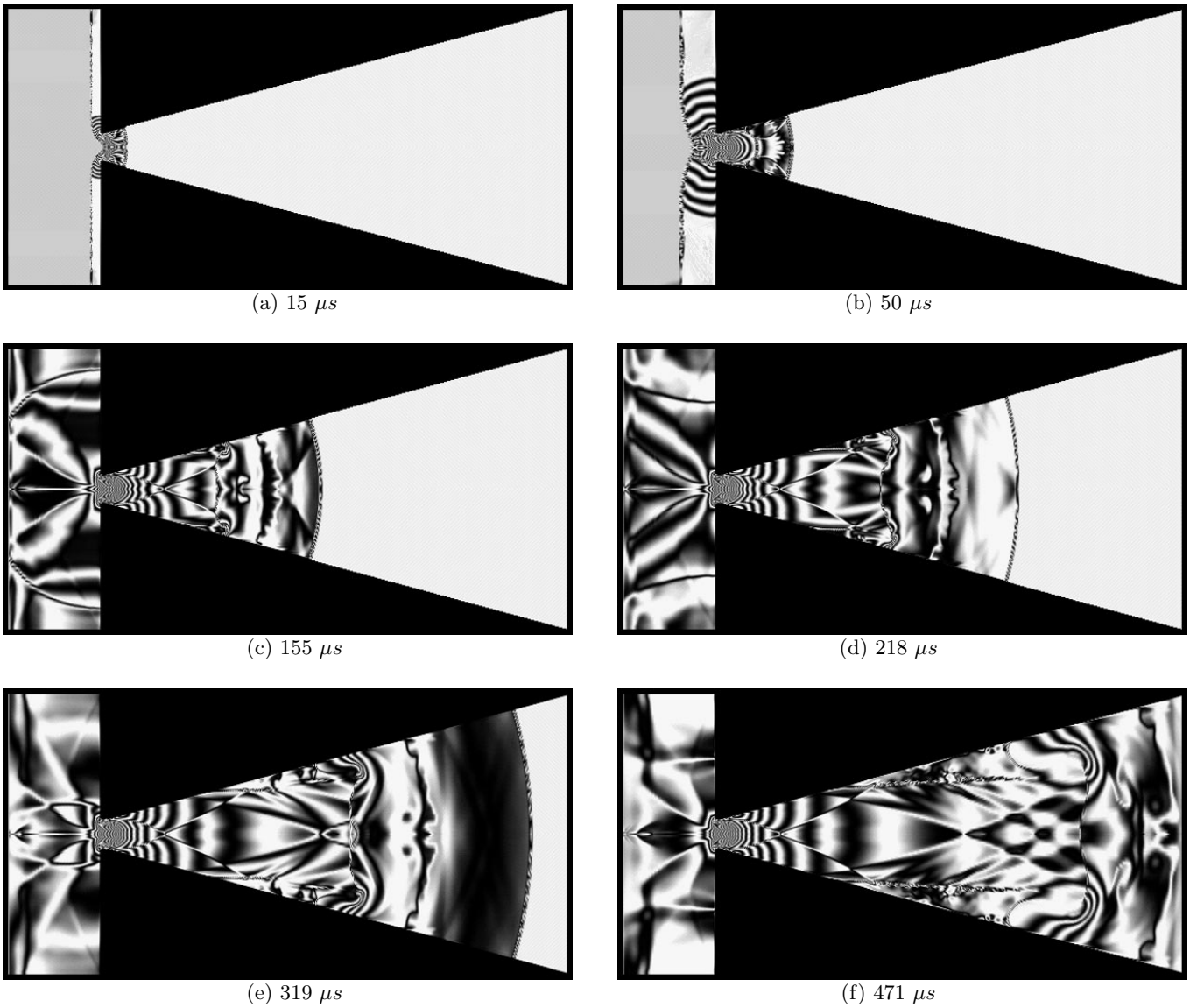

(a) 15 μs (b) 50 μs

(c) 155 μs (d) 218 μs

(e) 319 μs (f) 471 μs

Fig. 8a–f. Numerical results (implicit calculations)

number in strongly unsteady flows such as the current problem, the Reynolds number estimated from the conditions behind the incident shock wave and the distance fromt the primary shock wave to the secondary shock wave is about 8×10^5 at the time 218 μs. This value usually is considered for turbelent flows and it may apply to the current study as well.

It is noted that the numerically obtained interface is corrugated while the experimental picture shows smooth interface. This is considered to be the result of accumulation and propagation of numerical error created at the nozzle axis. As mentioned before, the numerical calculations are carried out for one half of the nozzle area by treating the nozzle axis as a solid wall. It is suspected that the combination of the boundary conditions and the grid distribution around the axis produces some numerical error which accumulates and become visible on the interface.

Figure 8 shows the numerical results of LUSGS scheme. Comparing Fig. 8 with Fig. 6, it is seen that the difference between the two are negligibly small. Although numerical fluxes in the explicit part of the LUSGS are evaluated with the same scheme as in the explicit calculations of Harten and Yee, this good agreement between the two is much more than expected if we consider the quite different solution processes of the two numerical schemes. It is also found that LUSGS scheme converges without viscous Jacobian terms and provides the same resolutions as the explicit Harten-Yee TVD scheme. This helped to reduce CPU time for LUSGS calculation since no matrix inversion was necessary.

Calculations are carried out for 473 μs from the moment when the incident shock wave arrives at the nozzle throat. It took 5 hours and 29 minutes CPU time for the explicit scheme and 4 hours and 18 minutes for the implicit scheme. The CFL number used for the ex-

plicit and implicit schemes are 0.8 and 20, respectively. Both schemes are optimized for Cray C90 supercomputer system with reasonable amount of efforts except that the computations are carried out for all grid points at each time step although the region ahead of the primary shock wave is not needed to be calculated.

The difference in the CPU time is not much between the implicit and explicit schemes for the present study of unsteady flow problem since the time step is limited more from the physical restriction than from numerical stability. Although no extensive investigations were done on the optimization of the time increment and the number of Newton iterations for LUSGS scheme, it is probably possible to reduce the number of Newton iteration by half without too much degradation in the resolution of numerical results. It may also be possible to increase the CFL number in LUSGS calculations more except at the beginning of the calculations. Even then, however, the difference in the CPU time is not so large as in usual cases of steady flow calculation. Considering the complex coding which makes implementations of sophisticated physical models such as turbulence more difficult and the sensitive optimization for combinations of operational parameters such as CFL number and numbers of iterations for each time step, the LUSGS implicit scheme is not so beneficial to use for such nonstationary problems as the current problems.

In order to simulate whole process of initiation of nozzle flow, it is now clear that the implementation of turbulence model in the numerical calculations is necessary. Considering the complex unsteady wave interactions, it may also be expected that the shear stress inside the flow field away from the nozzle wall play some significant role. In continuing numerical simulations of nozzle flow by taking these effects into account, it is expected that the unstructured mesh code with the grid adaptation is more suitable than the code with fixed structured grid and such a code is now being developed.

5 Conclusions

The starting process of a two-dimensional nozzle flow were calculated by explicit scheme of Harten-Yee TVD scheme and by implicit scheme of LUSGS. The numerical results are compared with the experimental results. It is found that the agreement between numerical results and those from experiment is good until the boundary layers become turbulent. It is, therefore, important to include the turbulence in the numerical simulations. Although LUSGS implicit scheme provides solutions with the same quality as the explicit TVD scheme with less CPU time, it may not so advantageous to use for strongly nonstationary flows such as the present nozzle starting process. Time steps in the numerical simulations are determined more from the nonstationary nature of the flow than from the stabilitys of numerical codes.

An unstructured code with grid adaptation is now being developed so that the effect of shear stresses not just at the wall but anywhere in the flow can be taken automatically. It is hoped that this new code with an appropriate turbulence model will become a good simulation tool for our experimental equipments.

References

Amann HO (1968) Vorgänge beim Start einer ebenen Reflexionsdüse. Thesis University Karlsruhe, Germany

Amann HO (1969) Experimental study of the starting process in a reflection nozzle. The Physics of Fluids Supplement I:I-155–I-153

Amann HO (1971) Vorgänge beim Start einer ebenen Reflexionsdüse. Zeitschrift für Flugwissenschaften 19 (Heft 10), 393–406

Anderson DA, Tannehill JC, Pletcher RH (1984) Computational fluid mechanics and heat transfer. Hemisphere publishing corporation, New York, NY USA

Harten A (1983) High resolution schemes for hyperbolic conservation laws. J. Comput. Phys. 49:357–393

Kano S, Yamamoto S, Daiguji H (1995) An efficient CFD approach for simulating unsteady hypersonic shock-shock interference flows. A Collection of Technical Papers, Sixth International Symposium on Computational Fluid Dynamics, Lake Tahoe, Nevada USA, Vol.2:570–575

Mark G (1958) The interaction of a reflected shock wave with the boundary layer in a shock tube. NACA TM 1418

Prodromou P, Hillier R (1992) Computation of unsteady nozzle flows. "Shock Waves" Proc. of the 18th Inter. Symp. on Shock Wave, Sendai, Japan, Vol.II:1113–1118

Roberts GO (1971) Computational meshes for boundary layer problems. Proc. Second Int. Conf. Num. Methods Fluid Dyn., Lecture Notes in Physics, Vol. 8, Springer-Verlag, New York:171–177

Smith CE (1966) The starting process in a hypersonic nozzle. J. Fluid Mech., Vol.24, part 4:625–640

Strang G (1968) On the construction and comparison of difference schemes. SIAM J. Numer. Anal., 5(3):506–517

Yee HC (1987) Upwind and symmetric shock-capturing schemes. NASA TM 89464

Yoon S, Jameson A (1988) Lower Upper Symmetric-Gauss-Seidel methods for the Euler and Navier-Stokes equations. AIAA J., Vol.26, No.9:1025–1026